Investigation into stress transfer characteristics in alumina-fibre/epoxy model composites through the use of fluorescence spectroscopy

H. MAHIOU
Manchester Materials Science Centre, UMIST/University of Manchester, Grosvenor Street, Manchester M1 7HS, UK; Laboratoire de Recherches et Applications en Mécanique Avancée, IFMA-B.P. 265-F63175 Aubière Cedex, France

A. BEAKOU
Laboratoire de Recherches et Applications en Mécanique Avancée, IFMA-B.P. 265-F63175 Aubière Cedex, France

R. J. YOUNG
Manchester Materials Science Centre, UMIST/University of Manchester, Grosvenor Street, Manchester M1 7HS, UK
E-mail: robert.young@umist.ac.uk

In composite materials, fibre/fibre interaction phenomena due to fibre failure are crucial in determining the composite fracture behaviour. Indeed, the redistribution of stress from a failed fibre to its intact neighbours, and stress concentration induced in the neighbouring fibres, determine the extent to which a break in one fibre will cause more breaks in others. In this paper, we have used fluorescence spectroscopy to study the stress transfer and redistribution induced by fibre fracture in two-dimensional Nextel-610 fibres/epoxy-resin micro-composites. The stress along the fibres was mapped at different load levels, and specimens with different inter-fibre distance were used to study the fibre content effect. The interfacial shear stress distribution along broken and intact fibres was derived by means of a balance of shear-to-axial forces argument. The experimental stress concentration factors (SCF) were smaller than values predicted from our model based on the cell assembly approach. As expected the 2D configuration allows access to the upper bound of the SCF in real composites. For the several specimens tested, a region of matrix yielding was observed behind the fibre fracture and no-debonding at the interface was detected. The measured SCF values agree well with those reported in recent study for carbon-fibre/epoxy model composites. © *1999 Kluwer Academic Publishers*

1. Introduction

It is now well established that the strength of fibre-reinforced composites is determined by the strength distribution of embedded fibres and the local stress distributions caused by fibre fractures. Both the stress build-up in a broken fibre and the magnitudes and local distributions of stress in the intact fibres are governed by the material properties and by the fibre-matrix interface [1, 2]. The complexities of the mechanisms of stress transfer and fibre stress redistribution, along with the statistical aspects of the fibre strength, make the modelling of the strength of fibrous composites a very difficult endeavour [2].

The problem of the local stress redistribution has been studied by a number of authors. Early models ignored the effect of material parameters and volume fractions and attempted to estimate a value of stress concentration factors (*SCF*) as function of single or multiple fibre fractures [3–5]. Other approaches, such as those by Fukuda and Kawata [6], Bader *et al.* [7] and recently Case *et al.* [8] yielded values of SCF as a function of material parameters and fibre volume fraction. Wagner and Eitan derived an analytical expression based on shear-lag analysis to estimate the SCF for a 2D microcomposite [9]. We have developed a model which allows the estimation of stress concentration factors as function of the material properties and of the fibre volume fraction. The model is based on the micromechanical model of cell assembly [10].

There are clearly a variety of theories predicting stress concentration factors in composites. Until recently, however, it was not possible to access the local stress field around fibre breaks experimentally. Current developments in Raman spectroscopy allow for the *in situ* mapping of local stress in a fibre and, hence, the determination of stress concentrations in real composites [2, 11–16].

Grubb *et al.* were able to measure the presence of stress concentrations in Nicalon/Kevlar and carbon/Kevlar 2D hybrid microcomposites [16]. In a recent study, Van den Heuvel *et al.* measured the stress concentration factors in carbon-fibre/epoxy-resin 2D microcomposites [14]. This work was followed by the study of Amer and Schadler on a graphite-fibres/epoxy-resin system [11].

In this paper, an experimental investigation into the influence of inter-fibre spacing on the stress transfer characteristics around fibre breaks, using the fluorescence spectroscopy technique, has been conducted on Nextel-fibres/epoxy-resin 2D-microcomposite models. First, we describe the experimental procedure followed for the specimens preparation and the materials used. The results and discussion are then presented for samples with several inter-fibre spacings.

2. Fluorescence and Raman spectroscopy
2.1. Fluorescence and Raman spectroscopy
When a monochromatic light beam, such as laser, hits a molecule three phenomena can happen: absorption, emission or scattering. The absorption phenomenon is the basis of the infra-red technique, whereas the emission is used in the fluorescence technique. The scattering phenomenon is the basis of the Raman technique.

With the development of laser technology providing an ideal monochromatic light source, laser Raman spectroscopy has found an increased use in the study of stress transfer in fibre-reinforced composites [2]. Over recent years, Raman spectroscopy has been used to investigate the stress redistribution in a number of systems including aramid-fibre/epoxy-resin and carbon-fibre/epoxy-resin microcomposites.
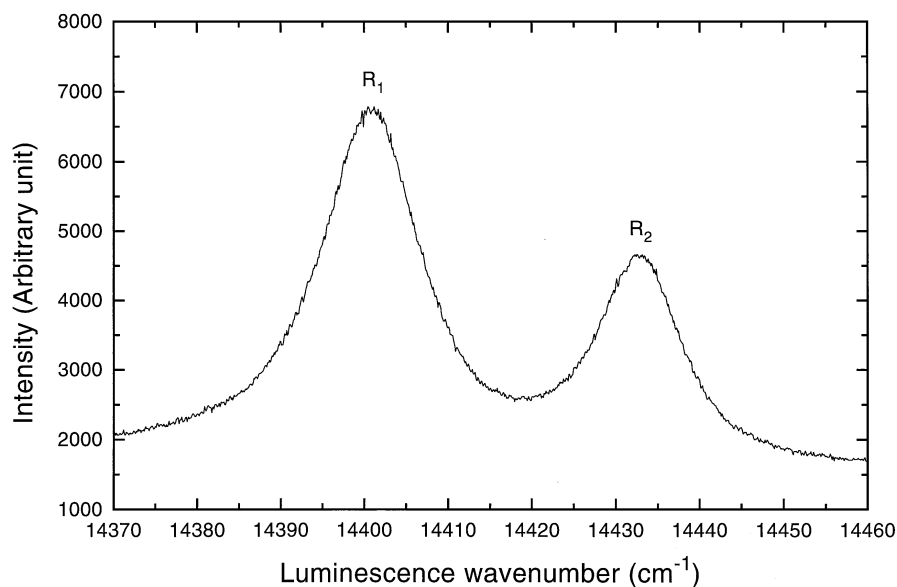
Figure 1 Luminescence spectrum of a Nextel 610 fibre.
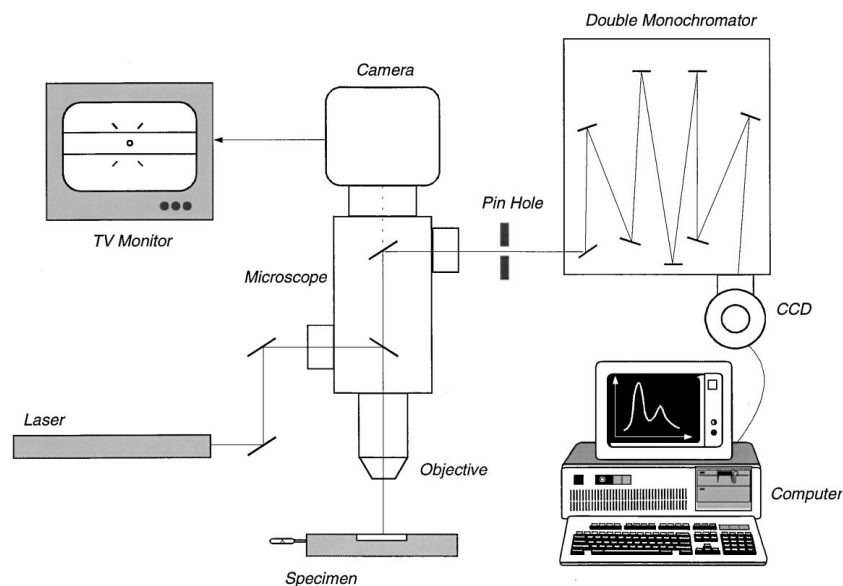
Figure 2 Schematic diagram of the Raman spectrometer.

In this experimental investigation of stress transfer characteristics, use is made of Nextel-610 fibres, which are relatively-pure polycrystalline α-alumina fibres, embedded in epoxy matrix. For this kind of fibre, fluorescence spectroscopy can be employed. The basis of the technique is that the characteristic luminescence of the fibre shifts with stress [18]. By using an optical microscope to define a probe of a few microns in diameter, the luminescence spectra can be obtained along the fibre. The observed shift in luminescence bands indicates the level of stress in the fibre.

The fluorescence of α-alumina fibres is due to the presence of Cr^{3+} impurities. These impurities give a doublet in the fluorescence spectrum, designated by R_1 and R_2 (Fig. 1), separated by about $30\,cm^{-1}$. The application of stress distorts the α-Al_2O_3 lattice and changes the energy levels involved in the electronic transition, thereby altering the R-band position [18].

The fluorescence signal is significantly more intense than a Raman signal and the band shifts are larger leading to more accurate analysis of fibre deformation.

2.2. Raman spectrometer
Fluorescence spectroscopy can be performed using an unmodified Raman spectrometer. In this study, use was made of a double Raman spectrometer (SPEX 1403)
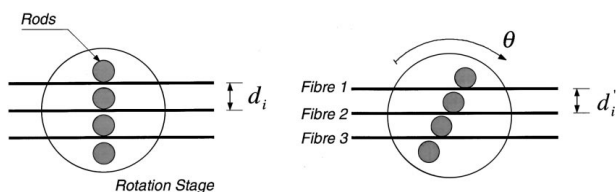
Figure 3 The multi-fibre specimen preparation: illustration of the principle for varying the fibre-to-fibre distance: assuming an original fibre inter-fibre distance d_i, a rotation θ of the fibre guides yields a new spacing $d_i' = d_i \cos \theta$ [20].
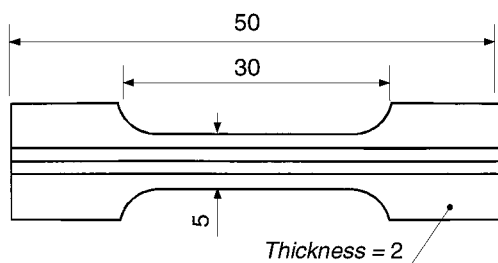
Figure 4 Schematic representation of dumb-bell shaped sample (Dimensions in mm).
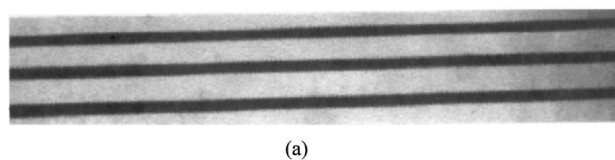
shown schematically in Fig. 2. It consists of the following parts:

1. *Light source:* Currently laser light sources are used in commercial Raman spectrometers due to the fact that they are highly monochromatic.

2. *Sample optics system:* In order to obtain high illumination of the sample and the efficient collection of the fluorescent radiation emitted from a small volume, the laser beam is polarised parallel to the fibre axis and focused on the fibre. The emitted fluorescence is collected by the microscope objective lens and passed to the monochromator entrance slits through a set of lenses.

3. *Monochromator:* Raman spectrometers use single, double or even triple monochromators to discriminate adequately between the fluorescence and the exciting radiation which also enters the instrument.

4. *Detector:* The light leaving the exit slit of the monochromator is collected and focused onto a Charge-Coupled Device (CCD) camera.

5. *Monochromator control and data collection system:* Usually a computer system and an interface between the computer and monochromator are used for control and data collection.

3. Experimental
3.1. Materials
The fibres used in this study were Nextel-610 fibres supplied by the company 3M, Minesota, USA. The fibres are relatively pure α-alumina fibres and have a poly(vinyl alcohol) sizing. They have an effective diameter of 12.8 μm and Young's modulus and tensile strength values of 380 and 1.61 GPa, respectively [18]. The fibres in this present study were utilised in their as-received condition, and no attempt was made either to remove or modify the surface sizing treatment.

The resin used was the two-part LY-HY 5052 (both supplied by Ciba-Geigy): Araldite® resin. The ratio of resin to hardener was $100 : 38$ by weight. The resin was cured at room temperature for 24 h and post-cured at 80 °C for 8 h. The resin has a tensile modulus of 3.0 GPa and a shear yield stress of 43 MPa [19].

3.2. Specimen preparation
Multi-fibre samples were prepared by positioning 3 fibres parallel at a predefined inter-fibre spacing using the technique developed by Wagner and Steenbakkers and Van den Heuvel [20, 21]. In this technique, use is

(a)
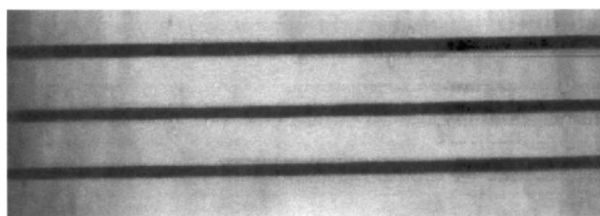
(b)

Figure 5 Photomicrographs showing model composites with three 12.8 μm diameter Nextel fibres separated by approximately (a) 2.6 and (b) 5.4 fibre diameters.

made of a fibre aligning device as shown schematically in Fig. 3. It consists of the following parts:

- *two rotation stages*, on which the fibres guides are fastened,
- *two fibre guides*, with stages that are able to rotate. The inter-fibre spacing can be adjusted by rotating the positioner to an angle θ (see Fig. 3),
- *two teflon rods*, that are held horizontally on stands and contain slots for each fibre, and are used to keep the fibres in position on the outside of the two guides,
- *mould supporting stage* which can move the mould up and down.

Three Nextel monofilaments were carefully extracted from a bundle and each fibre was guided in two corresponding slots on either side of the aligning apparatus. A weight of 100 mg was attached to each fibre to hold the monofilament in position. Then, by rotating the slots the inter-fibre distance was adjusted. In the experiments three inter-fibre distances were used (the inter-fibre distance is an average and is indicated in terms of the fibre diameter ϕ_f):

- large inter-fibre distance ($12.3\phi_f$),
- intermediate inter-fibre distance ($5.4\phi_f$),
- small inter-fibre distance ($2.6\phi_f$).

After the inter-fibre distance was adjusted, the next step was to embed the fibres in epoxy. A silicone rubber mould was placed underneath the fibres on the mould supporting stage. The stage was raised, lifting the mould until the fibres were at the centre of the half-depth of the mould. The fibres were glued in the cavity of a dumbbell shaped silicone mould using fast-setting epoxy cement. Subsequently, degassed epoxy resin was carefully injected into the mould gradually from one side to the other. Care was taken to avoid disturbing the fibres especially for the specimens with a small inter-fibre
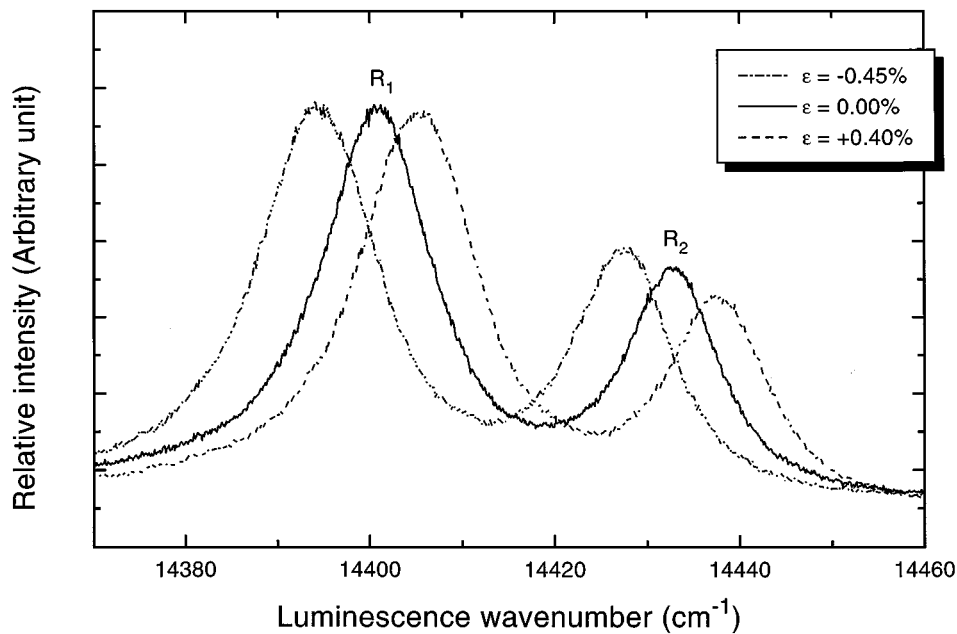
Figure 6 Shift in the position of the luminescence R bands with applied strain, ε, for a Nextel fibre.
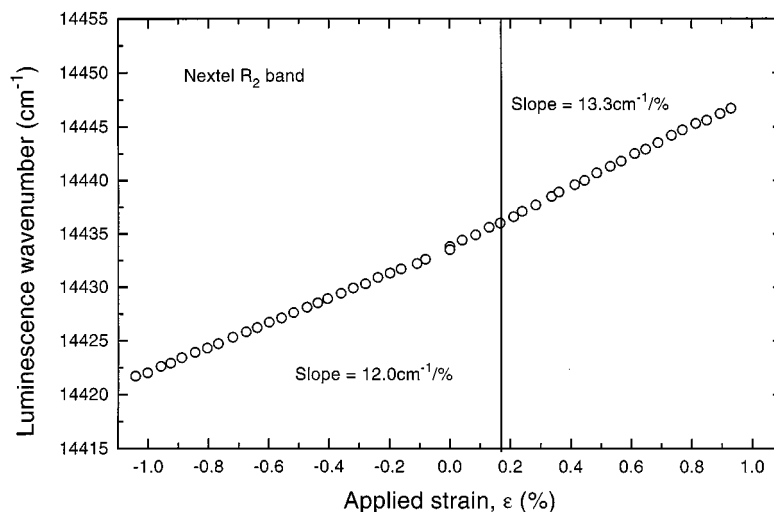
Figure 7 Variation of the wavenumbers of the luminescence R_2 band with applied strain for Nextel fibre [18].

distance. Finally, the samples were cured as described above. The cured specimens were then removed from the mould and polished with silicon-carbide paper (see Fig. 4 for the specimen dimensions). The inter-fibre distance was measured using an optical microscope in order to obtain an average inter-fibre spacing for each specimen.

Fig. 5a and b shows optical micrographs of specimens with three Nextel fibres separated approximately by 2.6 and 5.4 fibre diameters. It can be seen from Fig. 5 that the inter-fibre separations are uniform both along and between fibres. The main causes of any variations in inter-fibre spacing are the intrinsic crimps that cannot be removed fully under the small pre-load.

3.3. Fluorescence spectra acquisition

Luminescence spectra were obtained using an unmodified Raman microprobe system. It is based upon a SPEX 1403 double monochromator connected to a modified Nikon optical microscope. The luminescence spectra were obtained using the 632.8 nm line of a 15 mW He-Ne laser. Measurements were made using a $\times 50$ microscope objective lens giving an approximate beam size of 2 μm diameter and an intensity of about 1.0 mW at the fibre surface [18]. The set-up allows only the collection of the backscattered (180°) light. The spectra

Figure 8 Schematic representation of a microcomposite with a break in the fibre 2 ($x = 0$), surrounded by two intact fibres (referred as fibre 1 and fibre 3).

(a)

(b)
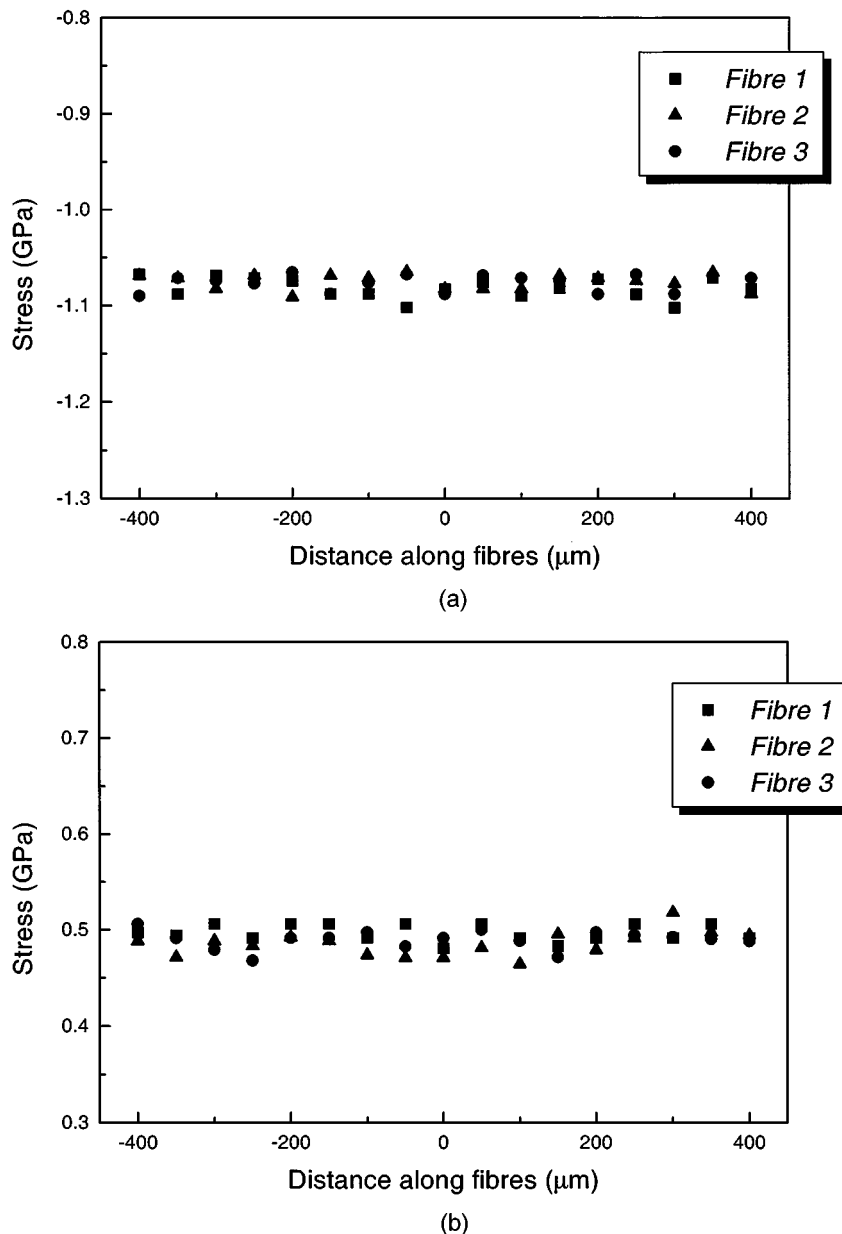
Figure 9 Stress profiles for a Nextel/epoxy microcomposite with large inter-fibre distance (12.3ϕ_f); the applied strain is (a) 0%, (b) 0.36%, (c) 0.68%. (*Continued*)

(c)
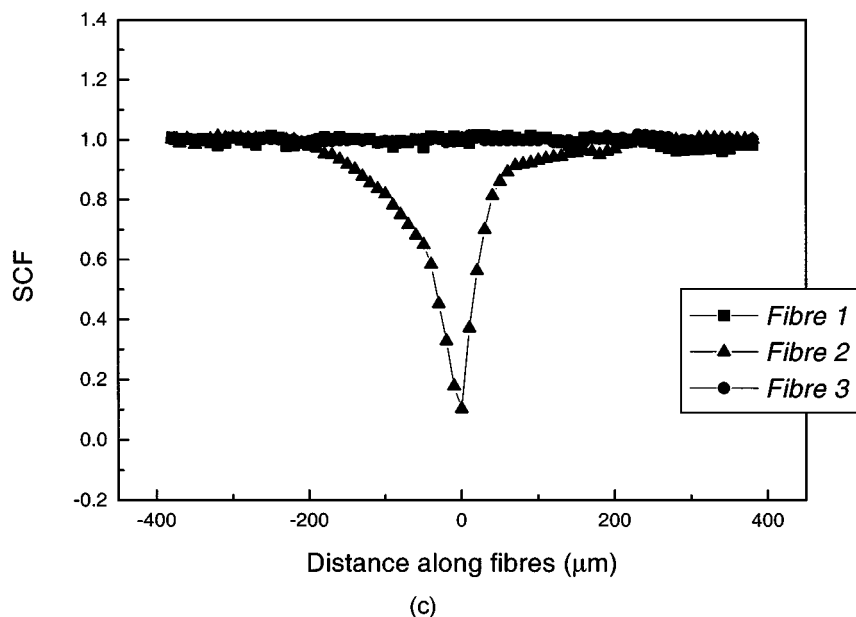
Figure 9 (*Continued*).

were recorded using a charge-coupled device (CCD) cooled with liquid nitrogen and kept at 145 K. The CCD was interfaced with a PC for data storage. The exposure time was set at 5 s. The fluorescence peak positions were determined by fitting the raw data with two Lorentzian curves.

3.4. Strain/stress calibration

In order to convert the shift of the fluorescence band into stress in the fibres, fluorescence spectra were obtained from Nextel fibres, bonded onto poly(methyl methacrylate) (PMMA) strips ($3 \times 10 \times 60$ mm) by a thin layer of PMMA, during deformation in a small four-point bending rig which fitted directly onto the microscope stage. The surface strain ($\equiv$ fibre strain) was measured using a resistance strain gauge bonded onto the PMMA strips surface. The strain was increased in steps of about 0.01% for both compressive and tensile deformation.

Fig. 6 shows luminescence R bands obtained from a Nextel fibre bonded onto a PMMA strip, in the unde-formed state, and subjected to compressive and tensile deformation. It can be seen that the peak positions of luminescence R bands for Nextel fibres are sensitive to the level of applied strain shifting to higher wavenumber in tension and lower wavenumber in compression. It was observed that the error in the measurement of the position of the R_2 fluorescence band was of about ± 1 cm^{-1} [18].

The variation of luminescence wavenumber for the R_2 band with applied strain is depicted in Fig. 7. It can be noticed that the luminescence R_2 band shifts approximately linearly with strain both in tension and compression. The behaviour is in fact slightly non linear and the data fall on a continuous curve as has been reported elsewhere by Yallee [18].

The band shift rate for the R_2 band in tension was found to be about 13.3 cm^{-1}/%. The fibre stress can be accessed by using the tensile Young's modulus of the Nextel fibres. Therefore, once the shift of the R_2 peak is measured, the fibre stress can be obtained from fibres under any general state of deformation.
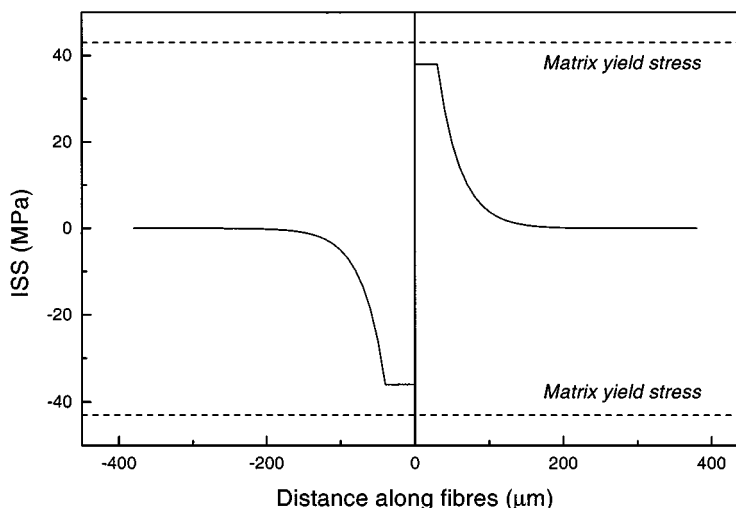
Figure 10 Derived interfacial shear stress along the broken fibre in Fig. 9c for the specimen with large inter-fibre distance.
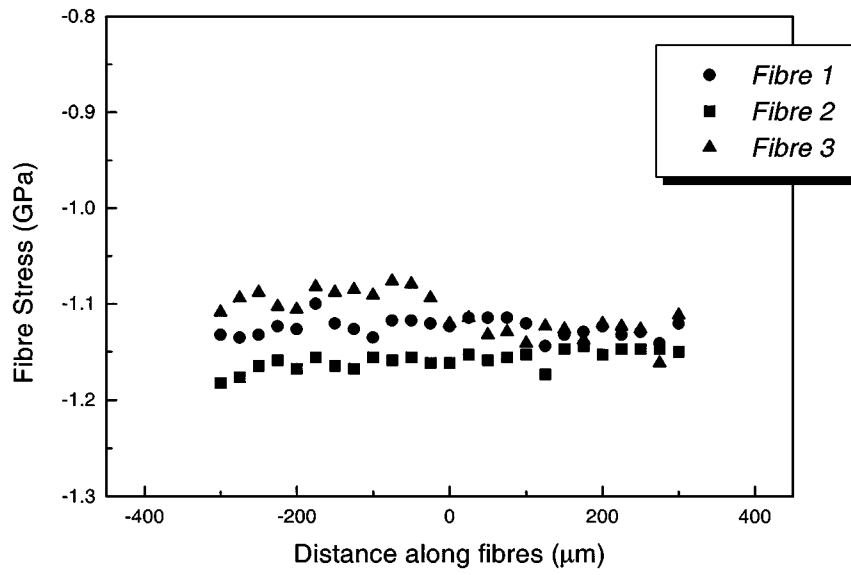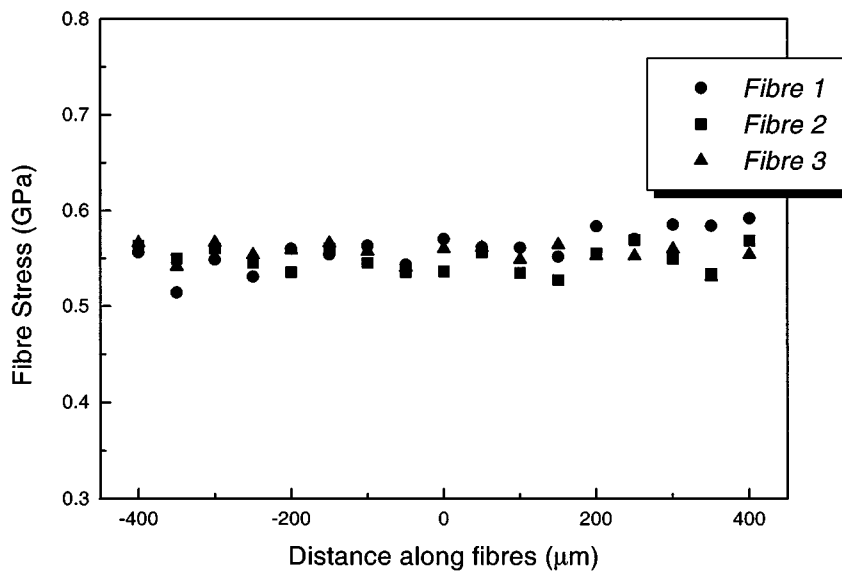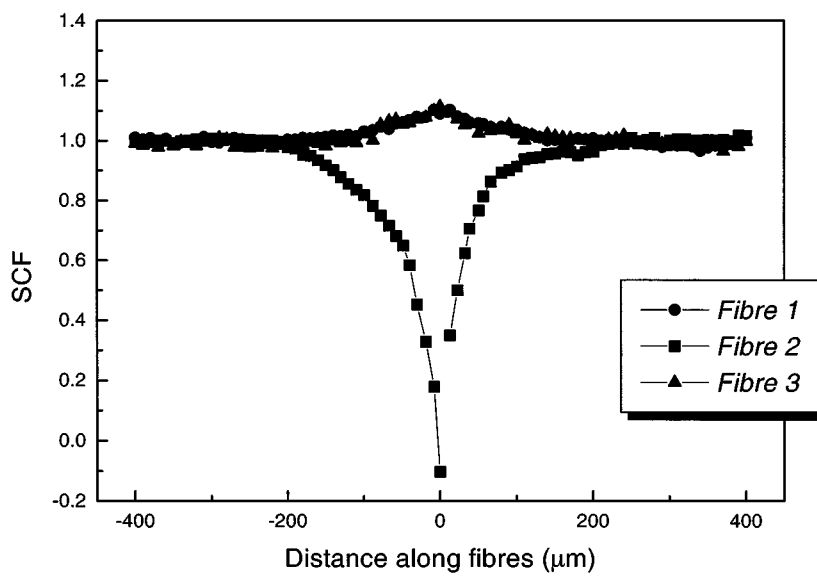
Figure 11 Stress profiles for a Nextel/epoxy microcomposite with intermediate inter-fibre distance ($5.4\phi_f$); the applied strain is (a) 0%, (b) 0.46%, (c) 0.75%.
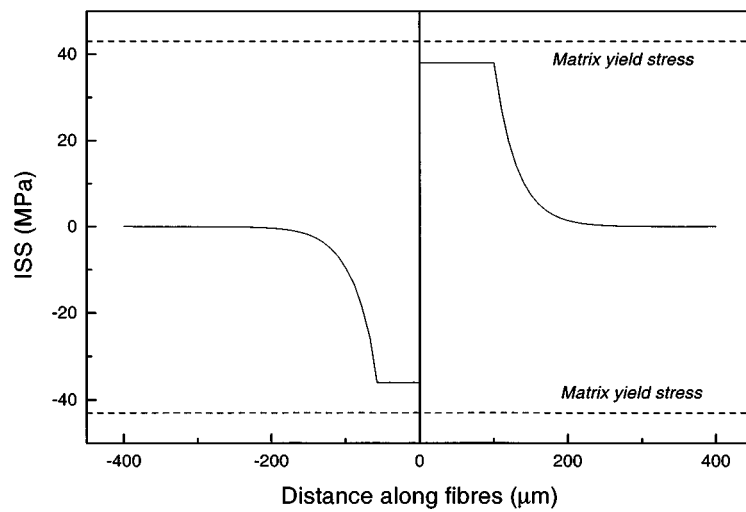
Figure 12 Derived interfacial shear stress for the broken fibre in Fig. 11c at an intermediate inter-fibre distance (5.4ϕ_f).
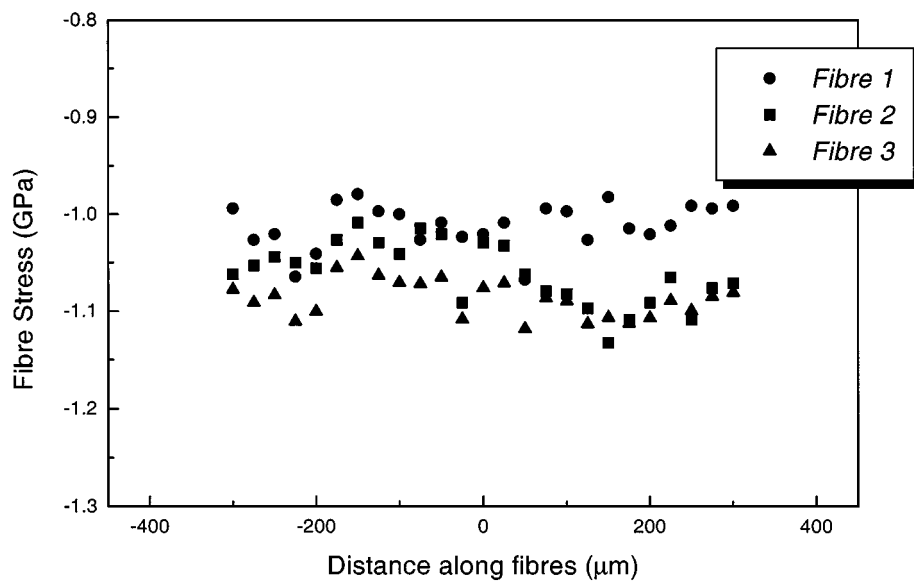
(a)
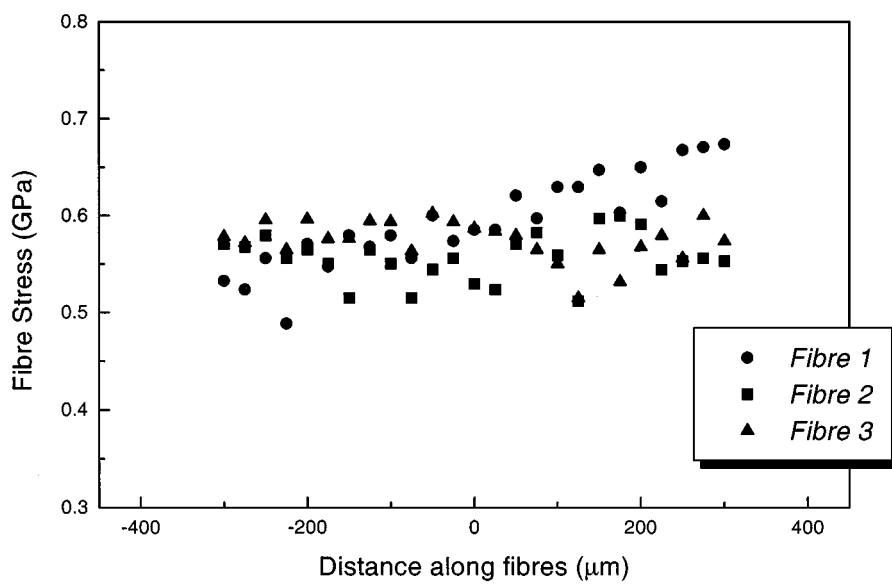
(b)

Figure 13 Stress profiles for a Nextel/epoxy microcomposites with small inter-fibre distance (2.6ϕ_f); the applied strain is (a) 0%, (b) 0.42%, (c) 0.72%. (*Continued*)

SCF

Distance along fibres (μm)
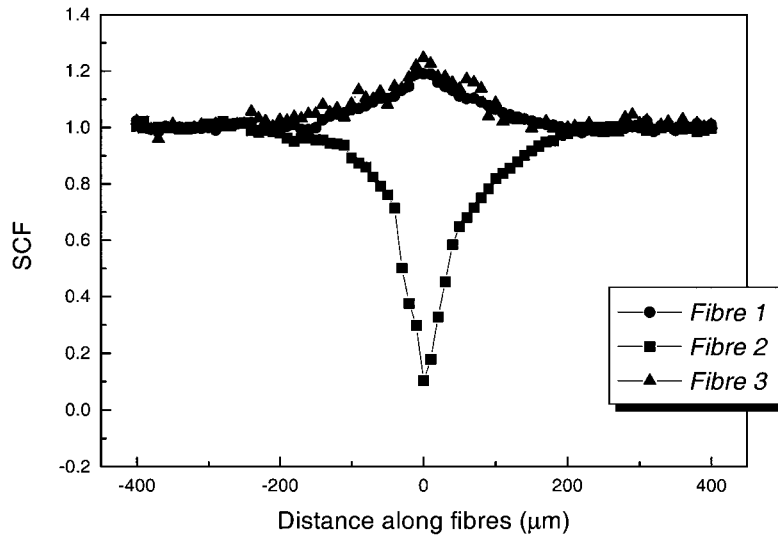
(c)

Figure 13 (Continued).

3.5. Stress mapping

Microcomposites with three inter-fibre distances ($2.6\phi_f$, $5.4\phi_f$ and $12.3\phi_f$) were produced and the stress profiles along a length of $1000\,\mu m$ of each fibres making up the samples were recorded at increasing strain levels. The samples were loaded incrementally using a Minimat straining rig which was placed on to the stage of the Nikon microscope. A strain gauge was attached onto the resin surface in order to obtain measurements of the strain applied to the sample.

Prior to the fibre fracture, spectra were taken at $50\,\mu m$ intervals. Mapping of the fibre stress prior to fibre fracture was undertaken to ensure that the fibre stress closely follows the applied strain. Once a single fibre fracture was observed, the measurements were taken at $10\,\mu m$ intervals in the vicinity of the break, at $20\,\mu m$ intervals further away from the break, and at $50\,\mu m$ intervals far away from the break. In all figures displayed in the next section, the fracture position along the fibre length is referred as $x = 0$. The broken fibre was referred as *fibre 2* and the two intact neighbouring fibres were designated by *fibre 1* and *fibre 3* (see Fig. 8).

The fibre stress profiles were converted into interfacial shear stress distributions (ISS) by calculating the derivatives from the equations of best fit of the stress profiles and deriving values of ISS by employing force balance acting upon the fibres and the interface [2]:

$$\tau = \frac{\phi_f}{2}\frac{d\sigma_f}{dx} \qquad (1)$$

In the fitting procedure, continuity of shear stress was imposed. The stress concentration profile was determined by fitting a Gaussian distribution function to the stress profile of a fibre adjacent to a broken fibre. Subsequently the shear stress profiles along adjacent fibres were derived using Equation 1.

4. Results and discussion

Figs 9, 11 and 13 show the variation the fibre axial stress with distance along fibres in the microcomposites with large, intermediate and small inter-fibre distance respectively at various strain levels (the strain levels are indicated in each figure).

4.1. Before fibre fracture

In Figs 9a, 11a and 13a the variation of the stress profiles along the fibres at the zero strain level are displayed for the various samples. For all the specimens produced, an initial compressive stress of about 1.1 GPa can be seen. The initial stress is expected to develop during cooling of the composite from the processing temperature of $80\,^{\circ}C$ due to the mismatch of thermal expansion coefficients between the matrix and fibre. A similar compressive stress for alumina-fibre/epoxy system has been reported elsewhere [18]. The values of residual stresses measured were also consistent with Nairn's analysis [18, 23]. Thus the application of stress must first of all overcome the initial compressive stress in the fibres before subjecting these to tension. As the strain is increased to 0.37, 0.46 and 0.42% for the specimens with large, intermediate and small inter-fibre distance, respectively, the stress in fibres increases and becomes greater than zero, i.e. the fibres are in tension (see Figs 9b, 11b and 13b). It can be seen that the stress levels in the three fibres for each specimen are all equal in magnitude.

4.2. After fibre fracture

At $\varepsilon = 0.68\%$ and 0.72%, a break is observed in the middle fibre (referred as fibre 2, Fig. 8) for the large ($12.3\phi_f$) and small ($2.6\phi_f$) inter-fibre distance (Fig. 9c and 13c). For the sample with intermediate inter-fibre distance ($5.4\phi_f$), a break is observed at a matrix strain level of 0.75% (see Fig. 11c). Raman spectra were obtained in the vicinity of the break as described above. The stress distribution in both the fractured and the intact fibres could therefore be obtained. Thus, single measurements at the vicinity of the fracture could yield: (a) *the ineffective length*, (b) the *interfacial shear stress*

distribution in the fractured fibres, in addition to (c) *the positively affected length* and *the stress concentration factors* in the adjacent intact fibres.

Fig. 9c shows the stress profiles along the length of the broken and the unbroken fibres for the specimen with a large inter-fibre distance. It can be seen that the fibre stress drops to zero at the tip of the fibre break and then builds-up from either side to reach the maximum value of fibre stress at a distance of approximately 250 μm. This length has been termed half of the ineffective length. Furthermore, Fig. 9c clearly shows that over approximately 50 to 70 μm around the break, linear stress build-up take place with a maximum interfacial shear stress around 38 MPa (Fig. 10). This shear stress is close to the shear yield stress of the epoxy-resin and hence, it is concluded that local yielding at the interface occurs behind the fibre break.

For the specimen with large inter-fibre distance no magnification of the stress level in fibre 1 and fibre 3 can be seen (Fig. 9c). This suggests that at this inter-fibre spacing no measurable over-stress of the intact fibres exists. In contrast for specimens with small and intermediate inter-fibre distances, the fibres 1 and 3 show a magnification of stress levels as a result of load redistribution (Figs 11c and 13c).
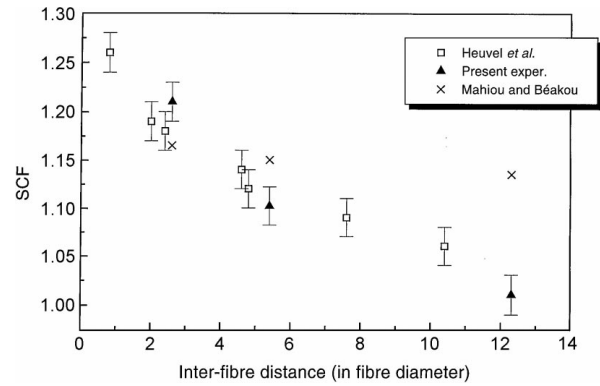
Figure 15 Stress concentration factors vs. the inter-fibre distance, comparison of the present measurements with Van den Heuvel's results [14] and the predicted values from our model [10].
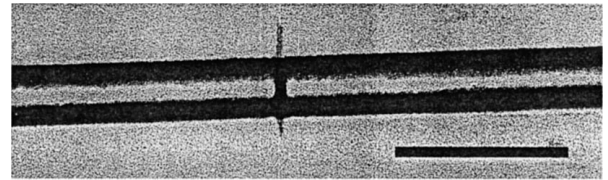
Figure 16 Matrix cracking around fibre break for the specimen with small inter-fibre separation (Scale bar 20 μm).
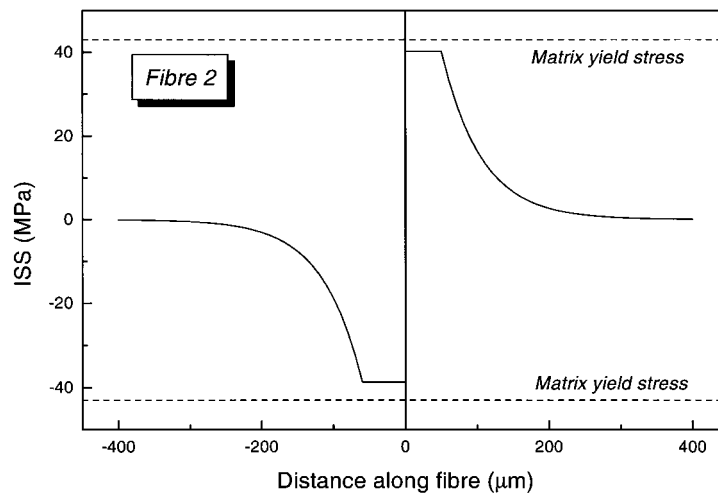
(a)
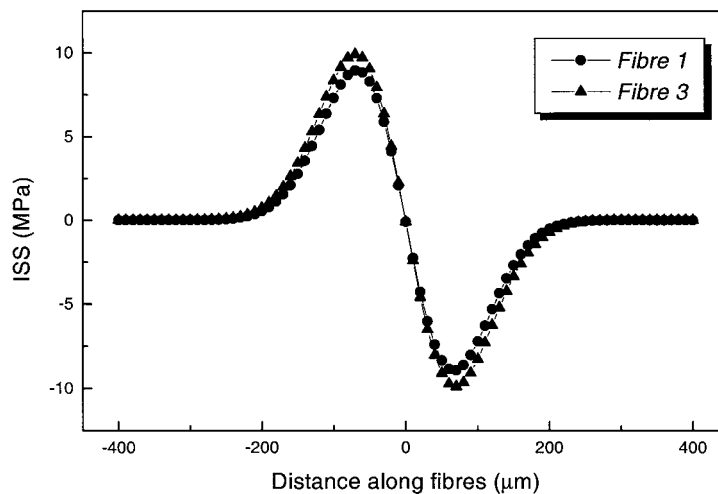
(b)

Figure 14 Derived interfacial shear stress for both: (a) the broken fibre in Fig. 13c, and b the adjacent intact fibre at small inter-fibre distance.
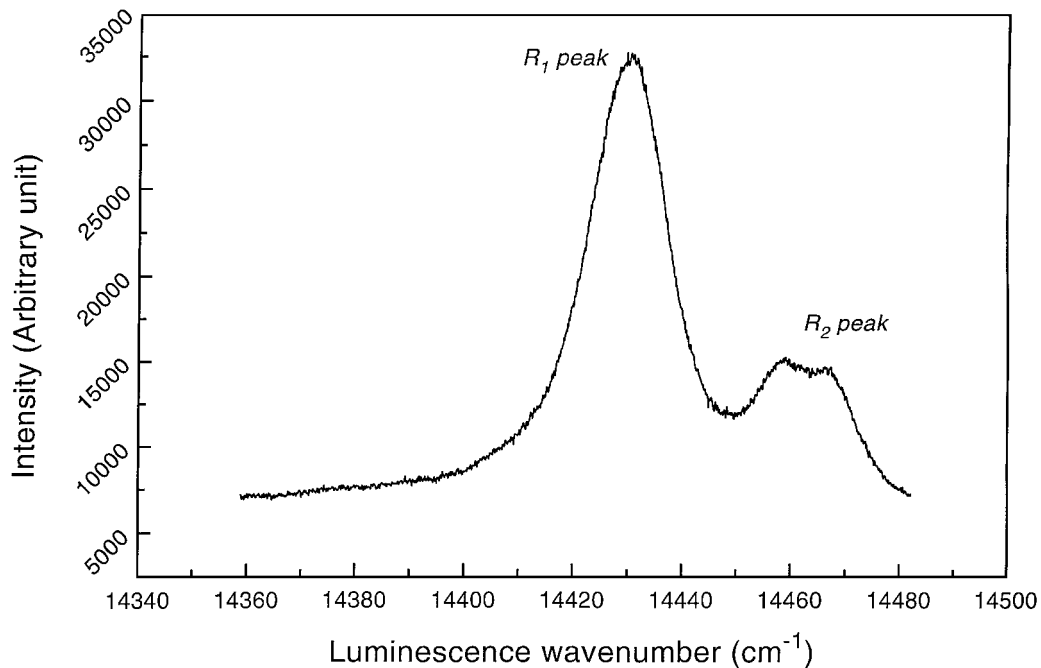
Figure 17 The fluorescence spectrum of Nextel-610 showing a broadening of the R_1 band and two peaks in the R_2 band in the vicinity of the fibre break.

It can be seen in Fig. 11c, that for the specimen with intermediate inter-fibre spacing, matrix yielding occurs over a length of about 90 μm (the stress builds-up linearly near the fibre break). The derived interfacial shear stresses are plotted in Fig. 12. The maximum of this stress occurs in the yielded region and decreases to 0 at $x = 250\ \mu$m. As can be seen in Fig. 11c, the axial stress near the fracture point was compressive and of the order of -0.3 GPa. As postulated in reference [13], the fibre may recoil back after fracture and the trajectory of stress change sign. Taking into account the residual tensile stress in the fibre at 0%, then the stored energy was high enough in magnitude to subject that part of the fibre to a compressive stress.

Fig. 13c shows that for the specimen with small inter-fibre spacing the stress profile builds-up linearly near the break over a length of about 50 μm, as for the specimens with large and intermediate inter-fibre distance. The derived shear stress in the broken fibre (Fig. 14a) suggest that local yielding occurs near the fracture. It is found that the ineffective length is around 500 μm, a value close to the one reported by Yallee [18].

Returning to the positively affected length, it is found that this length mirrors the ineffective length as assumed by Batdorf [24]. Similar conclusions can be made for the specimen with intermediate inter-fibre distance (see Figs 11c and 13c). The stress profile along the intact fibres is symmetrical and its maximum is situated in the rupture plane.

If we compare the stress profiles along the intact fibres for the specimens with $d_i = 2.60\phi_f$ and $5.4\phi_f$ (small and intermediate inter-fibre distance respectively), we notice a sharp decrease of the stress concentration factor along the length of the intact neighbouring fibres for the sample with small inter-fibre distance. This is may be due to a small matrix crack observed near the fracture point. For the specimen with $d_i = 5.4\phi_f$, no matrix cracking was observed near the break.

The shear stress profiles along the positively affected length are plotted in Fig. 14b for the specimen with small inter-fibre distance. The maximum shear stress is around 10 MPa. This value is close to the one reported elsewhere by van den Heuvel *et al.* for a carbon-fibre/epoxy-resin model composite at a similar inter-fibre distance [14]. It can be seen in Fig. 14b that the shear stresses acting upon the 2 intact fibres are similar in value. After following the fitting procedure described above, the maximum stress concentration factor was determined and was found to be 1.21 for $d_i = 2.60\phi_f$ and 1.10 for $d_i = 5.4\phi_f$.

As shown in reference [10], the SCF depends, for a fixed inter-fibre distance, upon the ratio E_f/E_m. For a carbon-fibre/epoxy-resin microcomposite ($E_f/E_m = 365/3$), van den Heuvel measured a stress concentration factor of 1.17 ± 0.02 at an inter-fibre distance of $2.6\phi_f$ [21] (see Fig. 15). This value is close to the one measured in our experiments. Any discrepancy could be due to ratio of the fibre to the matrix Young's moduli and to the small matrix crack observed near the fibre break (see Fig. 16). Indeed, the presence of a matrix crack is found to increase the stress concentration factor [21]. It was noticed however, that for the present composite system, the stress concentration factors decrease more rapidly with the inter-fibre distance than was found by van den Heuvel *et al.* [14].

For the Nextel-fibre/epoxy-resin composite ($E_f/E_m = 380/3$) with an inter-fibre distance of $2.6\phi_f$ our model [10] predicts a SCF of 1.165. As expected the 2D configuration of the micro-composites used experimentally allows access to the upper bound of the stress concentration factor. Indeed, our model [10] is based on square stitch arrangement of fibres and the stress concentration calculation is performed by two localisation computations in the vicinity of a fibre break. It can be seen in Fig. 15, that the predicted values from

the model tend asymptotically to 1.00 as the inter-fibre spacing increases.

It is interesting to note that, for the sample with a small inter-fibre distance, near the fibre break the fluorescence signal clearly shows two separate peaks for the R_2 band and in the same time the R_1 band broadens (Fig. 17). This is may be due to the crack in the fibre not being exactly perpendicular to the fibre axis. Similar observations have been noted for a carbon-fibre/epoxy-resin system [21] and were due to core/skin failure of the carbon fibres [21] reported widely in the literature [22].

5. Conclusions

It has been shown that fluorescence spectroscopy is a powerful tool to determine the stress transfer characteristics near a fibre break. The stress concentration factor, the ineffective length and the positively affected length can be measured by means of the band shift of the fluorescence spectrum. For a series of micro-composites having inter-fibre spacings varying from $2.6\phi_f$ to $12.3\phi_f$, the SCF was found to decrease from a value of 1.21 at an inter-fibre distance of $2.6\phi_f$ to a value approaching unity at high inter-fibre distance ($12.6\phi_f$). These values obtained agree with those reported by van den Heuvel et al. [14]. The measured values of the SCF have been compared to those calculated by our model. As expected the two dimensional configuration adopted for the micro-composites allows access to the upper bound of the stress concentration factors.

By using a balance-of-forces model, the fibre stress profiles have been converted to values of interfacial shear stress resulting in a determination of the local distribution of ISS. It has been observed that local matrix yielding of the interface occurs in the vicinity of fibre break. No debonding was observed for the three samples tested. It was found that the stress profile along the intact fibres is symmetrical and its maximum is situated in the rupture plane. The assumption made in Batdorf's model [24], used for the composite strength estimation, that the ineffective length mirrors the positively affected length has been proved experimentally.

References

1. H. MAHIOU and A. BÉAKOU, *Composites A* **29** (1998) 1035.
2. V. CHOHAN and C. GALIOTIS, *Comp. Sci. and Technol.* **57** (1997) 1089.
3. J. M. HEDGEPETH, *NASA TN D-882*, Langley Research Center, 1961.
4. J. M. HEDGEPETH and P. VAN DYKE, *J. Comp. Mat.* **1** (1967) 294.
5. D. G. HARLOW and S. L. PHOENIX, *ibid.* **12** (1978) 195.
6. H. FUKUDA and K. KAWATA, *Fibre Sci. Tech.* **9** (1976) 189.
7. M. G. BADER, R. L. SMITH and M. J. PITKETHLY, in Proc. Sixth Int. Conf. on Composite Materials (ICCM-6) and Second Europ. Conf. on Comp. Materials (ECCM-2), 20–24 July 1987, London, edited by F. L. Matthews, N. C. R. Buskell, J. M. Hodgkinson and J. Morton (Elsevier Applied Science, London, 1987) Vol. 5, p. 481.
8. S. W. CASE, G. P. CARMAN, J. J. LESKO, A. B. FAJARDO and K. L. REIFSNIDER, *J. Comp. Mat.* **29** (1995) 208.
9. H. D. WAGNER and A. EITAN, *Comp. Sci. Technol.* **46** (1993) 353.
10. H. MAHIOU and A. BÉAKOU, *ibid.* **57** (1997) 1661.
11. M. A. AMER and L. S. SCHADLER, *ibid.* **57** (1997) 1129.
12. C. MARTSON, B. GABBIATAS, A. ADAMS, P. MARSHALL and C. GALIOTIS, *ibid.* **57** (1997) 913.
13. A. PAIPETIS and C. GALIOTIS, *ibid.* **57** (1997) 827.
14. P. W. J. VAN DEN HEUVEL, T. PEIJS and R. J. YOUNG, *ibid.* **57** (1997) 899.
15. H. D. WAGNER, M. A. AMER and L. S. SCHADLER, *J. Mater. Sci.* **57** (1996) 1165.
16. Z.-F. LI, D. T. GRUBB and S. L. PHOENIX, *Comp. Sci. Technol.* **54** (1995) 251.
17. D. J. BANNISTER, PhD thesis, University of Manchester, Institute of Science and Technology, 1996.
18. R. B. YALLEE, R. J. YOUNG, *Composites A* **29** (1998) 1353.
19. M. C. ANDREWS, PhD thesis, Victoria University of Manchester, 1994.
20. H. D. WAGNER and L. W. STEENBAKKERS, *J. Mater. Sci.* **24** (1989) 3956.
21. P. W. J. VAN DEN HEUVEL, An experimental and numerical investigation into failure phenomena in multi-fibre microcomposites, PhD thesis, Technische Universiteit Eindhoven, 1998.
22. X. GU, R. J. YOUNG and R. J. DAY, *J. Mater. Sci.* **30** (1995) 1409.
23. J. A. NAIRN, *Mechanics of Materials* **13** (1992) 13.
24. S. B. BATDORF, *J. of Reinf. Plast. and Comp.* (1982) 153.